

Cronfa - Swansea University Open Access Repository

This is an author produced version of a paper published in:

Minerals Engineering

Cronfa URL for this paper:

<http://cronfa.swan.ac.uk/Record/cronfa43783>

Paper:

Li, T., Wu, A., Feng, Y., Wang, H., Wang, L., Chen, X. & Yin, S. (2018). Coupled DEM-LBM simulation of saturated flow velocity characteristics in column leaching. *Minerals Engineering*, 128, 36-44.

<http://dx.doi.org/10.1016/j.mineng.2018.08.027>

This item is brought to you by Swansea University. Any person downloading material is agreeing to abide by the terms of the repository licence. Copies of full text items may be used or reproduced in any format or medium, without prior permission for personal research or study, educational or non-commercial purposes only. The copyright for any work remains with the original author unless otherwise specified. The full-text must not be sold in any format or medium without the formal permission of the copyright holder.

Permission for multiple reproductions should be obtained from the original author.

Authors are personally responsible for adhering to copyright and publisher restrictions when uploading content to the repository.

<http://www.swansea.ac.uk/library/researchsupport/ris-support/>

Coupled DEM-LBM Simulation of Saturated Flow Velocity Characteristics in Column Leaching

Tao Li^a, Aixiang Wu^a, Yuntian Feng^b, Hongjiang Wang^a, Leiming Wang^{a*}, Xun Chen^a, Shenghua Yin

^a School of Civil and Resource Engineering, University of Science and Technology Beijing, Beijing 100083, China

^b College of Engineering, Swansea University, Swansea, SA2 8PP, UK

ABSTRACT

Heap leaching is a process extensively used by the mining industry to recover valuable metals from low-grade ores. However, the flow of the solution in a heap leaching system is disordered, uncontrollable and difficult to predict. To investigate the velocity characteristics of saturated flows in column leaching under different conditions, a combined experimental and numerical approach was carried out in the current work. MRI (magnetic resonance imaging) technology was employed in the column leaching experiment and numerical simulations were performed by combining the discrete element method (DEM) with the lattice Boltzmann method (LBM) to predict the microscopic seepage velocity field in the leaching column. The fluid flow and solid particles were modelled by the LBM and DEM respectively, and the interfacial interaction between the fluid and the solids was resolved by the immersed boundary method (IMB). It was demonstrated that the maximum fluid velocity is positively correlated with irrigation rate and porosity. Moreover, the preferential flow mainly passes through the main seepage channel. Thus, the numerical model developed in the present work is a reliable prediction tool for understanding the regularities of mesoscopic seepage velocity distributions in column leaching processes.

Keywords

Discrete element method; Lattice Boltzmann method; Heap leaching; Magnetic resonance imaging; Saturated flow;

1. Introduction

Currently, the application of heap leaching technology is increasingly widespread in recovering value metals, especially gold and copper, from crushed ores due to its low cost, operational simplicity, short construction time, good performance and environmental advantages (Lin *et al.*, 2005; Petersen 2016). During heap leaching, reagents (acid, cyanide or ferric) need to migrate through pores and cracks to reach the relevant mineral phases by the process of leaching solution seepage, which is the key to the success of the heap leaching process. Compared to the alkaline leaching process (Yin *et al.*, 2018), the permeability and heap compaction of acid leaching is commonly reduced, resulting the formation of insoluble residues. The migration of the leaching solution in the ore heap, accompanied by particle compaction, mineral dissolution and fine particles transport, leads to changes in the mesoporous pore structure of the ore heap, which in turn affect permeability. On the other hand, changes of seepage, such as surface flow, preferential flow and channeling, may result in an uneven distribution of the leaching solution in the ore heap, which affects the extraction rate of the target minerals (Jivkov *et al.*, 2014). Hence, understanding the leaching solution velocity distribution is important to enhance the performance of heap leaching.

Many investigators have carried out both experimental and numerical research on heap leaching. As a state-of-the-art non-invasive technology, magnetic resonance imaging (MRI) has been used to describe the liquid distribution and position relative to those of solid ore, and changes in the flow patterns in the bed may be projected. The 3D MRI

* Corresponding author;

Mailing address: No.30 Xueyuan Road, Haidian District, Beijing 100083, China.

E-mail address: ustb_wlm@126.com (L. Wang).

technique has also been adopted to study the effect of liquid flowrate changes on heap hydrology and control parameters during the bioleaching process, such as ferrous ion oxidation (Videla et al., 2016). Experimental results have shown that an increase in flowrate causes an increase in the number of rivulets in the leaching column (Fagan et al., 2013; Fagan et al., 2015). In addition, 3D imaging technologies, such as X-ray computed tomography (CT) and positron emission tomography (PET), have also been applied in heap leaching (Miao et al., 2017; Wildenschild and Sheppard, 2013). Ghorbani et al. (2011) use X-ray CT for the 3D characterization of crack and mineral dissemination in sphalerite ore particles. Lin (2015) also utilized X-ray CT to investigate the leaching behavior of metal sulfide ores. Similar work can also be found in Godel (2013), Miao (2017), and Yang (2014). However, many factors may affect on the rate of leaching, including the irrigation rate and the geometric properties of the pore network structure, and thus make experiments in realistic conditions difficult to manage. Complexity and lack of predictability are the main characteristics of heap leaching experiments.

Computational modelling, on the other hand, has proved to be a fruitful alternative due to its low cost and controllability. For instance, computed fluid dynamic (CFD) and other modeling methods is utilized in the heap leaching process where the saturated (McBride et al., 2012) and unsaturated conditions (McBride et al., 2017) are considered, respectively. Recently, the lattice Boltzmann method (LBM) has become a popular numerical technique for the simulation of fluid flow dynamic problems with complex boundary geometries (Videla et al., 2008). In fact, the popularity of LBM is also due to its capabilities of incorporating molecular level interactions and additional physical complexities such as multiphase and multicomponent flow (Wang et al., 2013; Han et al., 2007; Galindo-Torres, 2013; Han and Cundall, 2011). The coupling of the X-ray microtomography (XMT) technique and LBM has also been used for porous structure reconstruction and determination of the fluid flow regime (Lin et al. 2010). Moreover, the discrete element method (DEM) is a numerical scheme that was originally developed for rock mechanics (Cundall, 1971 & 1974). This method has the advantage of simulating the interaction of large assemblies of distinct particles. Recently, the coupled DEM-LBM technique has become a well-established computational method for solving particle-fluid interaction problems (Han et al., 2007; Cui et al., 2012; Ke et al., 2017; Johnson et al., 2017). Hence, the DEM-LBM coupling technique may be applied to the understanding of heap leaching processes.

In this work, we present a column leaching experiment by using the MRI technology and applying the DEM-LBM model to simulate saturated flow in column leaching. The fundamental aspects involved in the DEM- LBM and its application for the analysis of the leaching column are also described. The data extracted from the corresponding experiment are used to validate the mathematical model and the numerical approach. The microscopic seepage velocity field is analysed, and the effects of irrigation rate and porosity on the seepage velocity field are investigated.

Nomenclature

c	damping coefficient	t	time, s
C	lattice speed, m/s	Δt	the discrete time step, s
D	particle diameter, m	Δt_{cr}	the critical time step
dx	lattice spacing, m	\vec{T}_h	total torque generated by the hydrodynamic torque, N•m
e_i	discrete velocity vectors	v_{max}	maximum fluid velocity
f	friction coefficient in the DEM calculation	ν	kinematic viscosity of the fluid, m ² /s
f_0^{eq}	equilibrium fluid density distribution functions in the 0th direction, kg/m ³	\vec{v}	linear velocity of particle, m/s
\vec{F}_c	total contact force on a solid particle, N	W	fluid domain width, m
\vec{F}_h	the drag force on an object, N		

		<i>Greek letters</i>
f_i^{eq}	equilibrium fluid density distribution functions in the i th direction, kg/m ³	
\vec{F}_g	gravity (body force), N	β a weighting function
H	fluid domain height, m	ε the local fluid/ solid ratio
I	moment of inertia, kg•m ²	$\vec{\omega}$ the angular velocity of particle, m/s
k_n	normal stiffness constant	ξ the critical damping ratio
k_t	tangential stiffness constant	δ the contact displacement, m
m	mass of a solid particle, kg	η the local contact natural frequency
n	porosity	
Q	irrigation rate, mL/s	ρ fluid density, kg/m ³
R	the radius of particle, m	ρ_p fluid density, kg/m ³
R_h	the ratio of hydraulic radius	τ dimensionless relaxation time

2. Numerical methods

2.1 Discrete element method for moving particles

The DEM overcomes the macroscopic continuity assumption of continuum mechanics and is a method of discontinuous medium mechanics. When particles are not directly in contact among them but are driven only by gravity (body force) and fluid flow, their motions can be determined by Newton's second law in the form of the following equations:

$$m \frac{d\vec{v}}{dt} = \vec{F}_g + \vec{F}_h \quad (1)$$

$$I \frac{d\vec{\omega}}{dt} = \vec{T}_h \quad (2)$$

where m and I denote respectively the mass and moment of inertia; \vec{v} and $\vec{\omega}$ represent the particle's linear velocity and angular velocity; \vec{F}_g is the gravity (body force), \vec{F}_h is the hydrodynamic force applied by the flowing fluid; \vec{T}_h refers to the total torque arising from the hydrodynamic torque. Those equations can be solved numerically by an explicit numerical integration, such as central difference scheme.

When taking into account all the forces acting on a solid particle, the dynamic equations of the discrete element can be symbolically expressed by the following equation (ignoring the equation for rotational motion for simplicity):

$$m \frac{d\vec{v}}{dt} + cv = \vec{F}_c + \vec{F}_g + \vec{F}_h \quad (3)$$

where c is a damping coefficient, v is the kinematic viscosity of the fluid and \vec{F}_c is the total contact force acting on single particle.

For the current problem, the linear normal contact model is given as

$$\vec{F}_c = k_n \delta \quad (4)$$

where k_n is the normal stiffness and δ is the overlap, the critical time step associated with the explicit time integration of (3) is given by

$$\Delta t_{cr} = 2(\sqrt{1 + \xi^2} - \xi)/\omega \quad (5)$$

where $\omega = \sqrt{k_n/m}$ is the local contact natural frequency and $\xi = c/2m\omega$ is the critical damping ratio.

2.2 Lattice Boltzmann method for incompressible fluid flow

Generally, the D2Q9 model is implemented in the solution of 2D incompressible fluid flows in the LBM. The entire fluid domain is divided into mutually orthogonal square lattices at first, with a lattice spacing of dx in both x and y directions. Then, the fluid phase is represented as aggregates of fluid particles located at each lattice node and moving with a discrete speed in a discrete direction at each time increment, as shown in Fig. 1. In the D2Q9 model, the nine discrete velocity vectors $e_i (i=0 \sim 8)$ are defined as follows:

$$e_i = \begin{cases} 0 & (i = 0) \\ C \left(\cos\left(\frac{\pi(i-1)}{2}\right), \sin\left(\frac{\pi(i-1)}{2}\right) \right) & (i = 1, 2, 3, 4) \\ \sqrt{2}C \left(\cos\left(\frac{\pi(i-5)}{2} + \frac{\pi}{4}\right), \sin\left(\frac{\pi(i-5)}{2} + \frac{\pi}{4}\right) \right) & (i = 5, 6, 7, 8) \end{cases} \quad (6)$$

in which C is defined as the lattice speed and given by $C = dx/\Delta t$, with Δt the discrete time step.

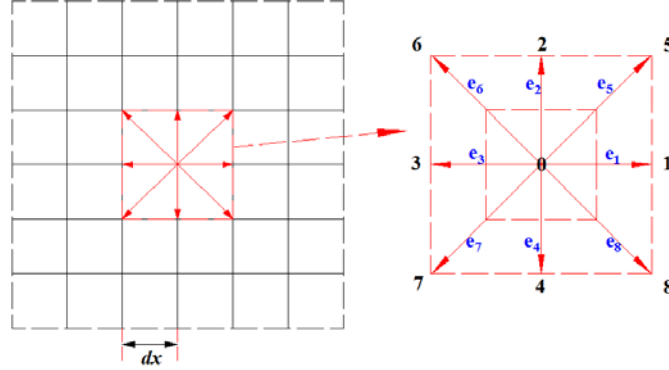


Fig. 1. Standard LBM lattice and D2Q9 model

$f_i(x, t)$ is the density distribution function with velocity e_i at position \mathbf{x} at time t , and its evolution governs the movement of fluid particles and can be written as,

$$f_i(x + e_i \Delta t, t + \Delta t) = f_i(x, t) - \frac{1}{\tau} [f_i(x, t) - f_i^{eq}(x, t)] \quad (i = 0, \dots, 8) \quad (7)$$

in which τ is the relaxation parameter and related to the viscosity of the fluid. $f_i^{eq}(x, t)$ is the equilibrium distribution function and is given by,

$$\begin{cases} f_0^{eq} = \omega_0 \rho \left(1 - \frac{3}{2c^2} \mathbf{v} \cdot \mathbf{v} \right) \\ f_i^{eq} = \omega_i \rho \left(1 + \frac{3}{c^2} e_i \cdot \mathbf{v} + \frac{9}{2c^2} (e_i \cdot \mathbf{v})^2 - \frac{3}{2c^2} \mathbf{v} \cdot \mathbf{v} \right) \quad (i = 1, \dots, 8) \end{cases} \quad (8)$$

in which ω_i are the weighting factors,

$$\omega_0 = \frac{4}{9}; \quad \omega_{1,2,3,4} = \frac{1}{9}; \quad \omega_{5,6,7,8} = \frac{1}{36} \quad (9)$$

The central issue in applying the coupled LBM-DEM approach involves the interaction between the fluid and particles or wall boundaries. The bounce-back technique (Feng et al., 2007; Han et al., 2007) is the simplest approach for modelling the interaction between a fluid and a solid by the LBM method and is usually suitable for simulating the interaction at stationary boundaries. It is assumed that the boundary between the wall and the stationary particle can be approximated as boundary points located at the middle of the connection between the solid and fluid nodes. The bounce-back technique enforces the no-slip condition at the fluid-solid interfaces by reflecting particle distribution functions from the boundary nodes in the direction of incidence, as shown in Fig. 2. Therefore, the solid and the fluid have the same speed at the boundary points.

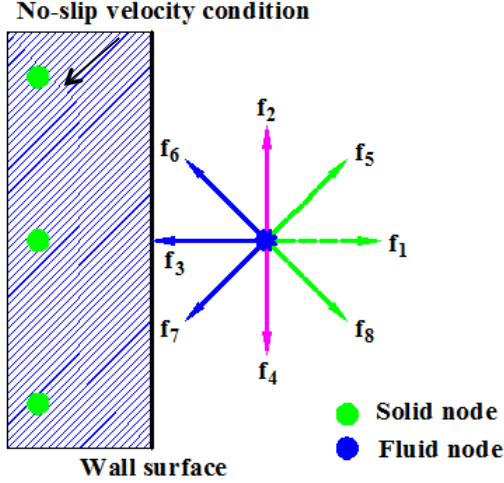


Fig. 2. Schematic diagram of LB bounce-back rule

2.3 Coupled DEM-LBM

To obtain an accurate and smooth lattice representation of moving particles and reduce the fluctuation of the computed hydrodynamic forces, the immersed moving boundary method (IMB), which was proposed by Noble and Torczynski (Noble et al., 1998), is adopted in this paper. A new parameter, the fluid/solid ratio ε , is introduced, which is the area fraction of the nodal cell covered by a particle, as illustrated by the magenta area in Fig. 3. In addition, V_s and V_p are the velocities of the solid node and the particle, respectively.

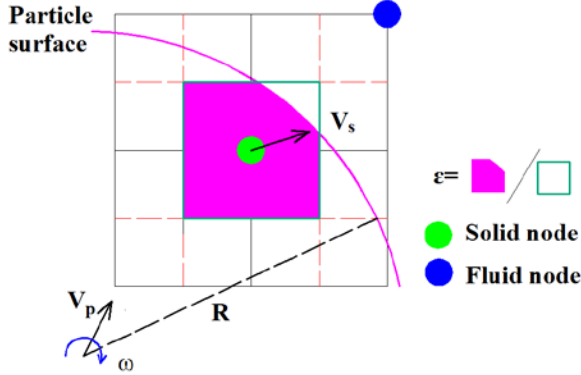


Fig. 3. Immersed moving boundary coupling scheme and definition of local solid ratio ε

Then the equation of the density distribution function for those lattice nodes fully or partially covered by a solid particle is modified to

$$f_i(x + e_i \Delta t, t + \Delta t) = f_i(x, t) - \frac{1}{\tau} (1 - \beta) [f_i(x, t) - f_i^{eq}(x, t)] + \beta f_i^m \quad (10)$$

where β is a weighting function depending on the local fluid/ solid ratio ε defined as the fraction of the node area

$$\beta = \frac{\varepsilon(\tau-1/2)}{1-\varepsilon+(\tau-1/2)} \quad (11)$$

Further details of the IMB method and the coupling of the LBM with the DEM, including an assessment of mixed boundary conditions in various flow geometries, can be found in the literature (Feng et al., 2007; Han et al., 2007; Peskin 2002; Owen et al., 2011).

3. Experiment

3.1 Materials

Self-made spheroidal agar beads (Fig. 1) were used to represent ore particles in the experiment, and the particle size distribution ranged from 8 mm to 12 mm. Because the shaped agar beads reduce the noise impact of metal magnetic substances, facilitate the capture of signals during the MRI scanning, and are low-cost and stable, we used agar balls instead of actual ores. Finally, the internal pore structure of the leaching heap was constructed according to the random packing distribution of agar beads.



Fig. 4. Spheroidal agar beads with different sizes

3.2 Experiment apparatus

In this work, the seepage velocity field experiment system mainly consists of three parts: a column leaching device, a clamping stabilizer and an MRI system, as shown in Fig. 5. The main body of the column leaching device is a homemade plexiglass column (60 mm inner diameter, 220 mm height). A buffered gravel layer and a sieve plate with uniform circular holes were installed at the top and the bottom of the column, respectively. Furthermore, the column imaging was performed on a 3.0 T Discovery 750 MRI system (GE Medical System, US), and FRFSE sequence and T1 FLAIR sequence were included. All images were acquired perpendicular to the axial plane with a slice thickness of 0.4 mm, a gap of 0.4 mm, and a field of view of 22 × 15 cm.

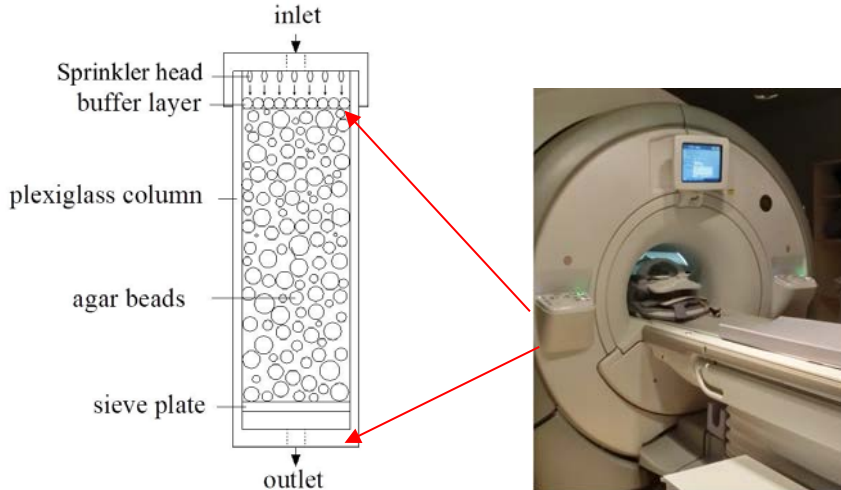


Fig. 5. The MRI Experiment system (At leftmost is shown the zoomed schematic view of the column leaching device)

3.3 Experiment procedure

- i) The agar beads with different particle sizes are mixed and placed in the plexiglass column. The column leaching device is subjected to saturated water for 2 hours to fully fill the pores in the column leaching system and exhaust the air inside the device.
- ii) The column leaching device is placed in the MRI system together with the clamping stabilizer for imaging experiments. Besides, the irrigation rate is set to 0.3 mL/s, 0.4 mL/s and 0.5 mL/s, respectively.
- iii) Images with clear outline, no artifacts and not distorted are saved for subsequent image processing and result analysis.

4. Numerical simulation conditions

As illustrated below, the rate of leaching is critically determined by several factors, including irrigation rate and particle porosity. The numerical simulation of the column leaching process was undertaken in similar fashion using the 2D LBM-DEM framework. A Hertzian contact penalty was employed to account for the contact between the beads, a pressure boundary condition was employed in the flow direction and non-slip boundary conditions were applied on the solid-fluid interfaces. The fluid domain was discretized with a D2Q9 lattice using a spacing of 0.0003, resulting in a grid size of 600×200 and approximately 1.2e05 grid nodes. Other parameters used in the numerical simulations are shown in Table 1.

Simulations are run under different influencing factors and but care is taken to ensure that the flow is under laminar conditions. In this work, three cases are carried out with three spraying intensities: 0.3 mL/s, 0.4 mL/s and 0.5 mL/s, and other three cases are performed with three different particle porosities: 20%, 25% and 30%. All the simulations are finished within 5 hours using a 64-bit computer with an Intel Xeon 3.60 GHz CPUs and 16.0 GB RAM. Under the condition of the spraying intensity at the inlet was 0.5mL/s. The numerical simulation results indicated that the maximum flow rates range from 1.70 cm/s to 2.0 cm/s.

Table 1. Parameters used in the simulations

Phase	Parameter	Symbol	Units	Values
Fluid	Domain height	H	m	0.18
	Domain width	W	m	0.06
	Lattice spacing	dx	m	0.0003
	LBM time step	Δt	s	1.0×10^{-4}
	Relaxation parameter	τ	-	0.55
	Fluid density	ρ	kg/m ³	1000
	Kinematic viscosity of the fluid	ν	m ² /s	1.0×10^{-5}
	Ratio of hydraulic radius	R_h	-	0.8
Solid	Particle diameter	D	m	0.08~0.12
	Particle density	ρ_p	kg/m ³	2500
	Friction coefficient in the DEM calculation	f	-	0.3
	DEM time step	dt	s	2.5×10^{-5}

5. Results and discussion

5.1 Preprocessing of MRI images

To capture the porous network structure of the packed leaching heap, which defines the geometric properties of the flow, the images obtained by MRI were subjected first to threshold processing and then binarization processing. The grey value of the pore portion in the heap is set as 0, where the pixel point is 0; the pixel point whose grey value is not 0 is set as 1. Fig. 6a shows a representative original grey-scale MRI image (longitudinal section), and Figs. 6b and 6c are the images after threshold processing and binarization processing, respectively.

As shown in Fig. 6c, the solid region is in black and the fluid is in white. It was observed that there are areas in the column without agar beads, which results from the plexiglass column not being completely filled with agar beads before the experiments. Comparing Fig. 6(a) with Fig. 6(c), it can be seen that the shapes of partial particles in the binarization processing image were not regularly circular. The reason for this phenomenon is that the slice thickness was 4 mm during magnetic resonance imaging, the dispersion of particle position changed the pixel value, and the points of the particles were separated after binarization processing. However, this change was within a reasonable range, and would not impact the subsequent analysis. In addition, the packed leaching column was saturated, and the

leaching solution occupied pores during imaging. Therefore, the distribution of the leaching solution also reflects the internal pore structure of the sample. In other words, the white region representing the aqueous leaching solution also indicates the distribution of intergranular pores in the binary image.

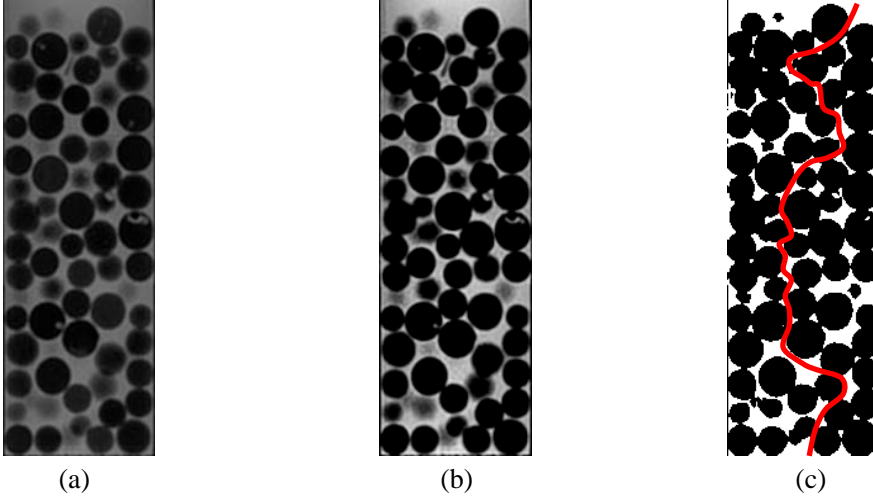


Fig. 6. Processing of the MRI data to phase map. (a) is MRI image, (b) is threshold image, (c) is the binary image. The red line in (c) is the main seepage channel. ($Q = 0.5 \text{ mL/s}$)

5.2 Microscopic analysis of seepage velocity field

The range of MRI imaging is the longitudinal section of the leaching column; hence, the 2D DEM-LBM coupling model can be used to analyse the distribution of seepage velocity field. One limitation of 2D leaching solution flow simulations, however, is the very low permeability of the structurally, discrete element field, as the well-developed network of particle-particle contacts forms a barrier impermeable to leaching solution percolation. To overcome this problem a contact buffer is incorporated into the discrete element contact which allows neighbouring particles to engage in contact before they physically bond. As shown in Fig. 7, the red dashed circles and the black solid circles represent the contact boundaries and the physical boundaries, respectively. The contact buffer for the circular particles is introduced as a reduction in the original boundary radius while the contact radius remains the same.

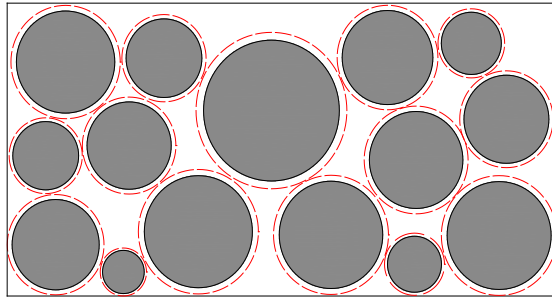


Fig.7. Schematic representation of the discrete element contact buffer applied to circular particles.

The red dashed circles represent the contact boundaries and the black solid circles represent the physical boundaries. It is possible to utilize the binary image directly as the input geometry of the problem in the LBM to conduct numerical simulations. The present work, however, takes a different approach in which the radii and positions of the particles are identified from Fig. 6(c), and used to reconstruct the particle packing in the leaching column. This packing is then employed in the LBM for the subsequent numerical analysis. This approach has an advantage over the image based LBM analysis in that the particle sizes can be altered later to represent different leaching porosities. Note that 2D LBM models used below approximately match the experiments that are 3D or approximately axi-symmetric in nature; therefore, there are differences between the numerical and experimental results. Although no

quantitative comparison was performed to quantify the numerical error, the 2D numerical results were reasonably expected to be able to represent the experiment well, as shown below.

Fig. 8 demonstrates the numerical leaching solution of the flow velocity distribution inside the leaching column for porosity $n = 35\%$ and irrigation rate $Q = 0.5 \text{ mL/s}$. It can be seen that the main seepage channel exists along the high flow velocity region in the longitudinal section. The location of particles in the DEM-LBM coupling models are generated according to the binary image, and the main seepage channel in Fig. 8 is in good agreement with the experimental result, which is given in Fig. 6(c) (the red line). Generally, the liquid is distributed in heaps via two mechanisms: downwards gravitational flow through the heap in larger channels and dispersion of the liquid under capillary forces in the unsaturated heap. In this study, the flow passes through a granular bed comprising spherical solid particles arranged randomly, which were driven by the upper pressure. The state of the main seepage channel in the longitudinal section, which is connected or blocked, affects the permeability and the leaching rate directly. Thus, the main seepage channel is significant for the flow of leaching solution between packed particles.

In addition, the packed leaching column contains intergranular pores, a fluid stagnant zone, a fluid transition zone, a fluid flow zone and pore throat. The zoomed view in Fig. 8 shows the fluid velocity vector profile where the vector lengths are relative to fluid velocity. From this profile, it is clear that the stagnant fluid is contained in the interstitial spaces between particles, and in the network of flowing fluid channels. Furthermore, the flow is driven in the outlet direction, and the fluid velocity increases when the fluid is close to the pore throat and the maximum fluid velocity ($v_{\max} = 2 \text{ cm/s}$) is obtained at the centre of the pore throat. In contrast, the fluid velocity decreases when it is away from the pore throat.

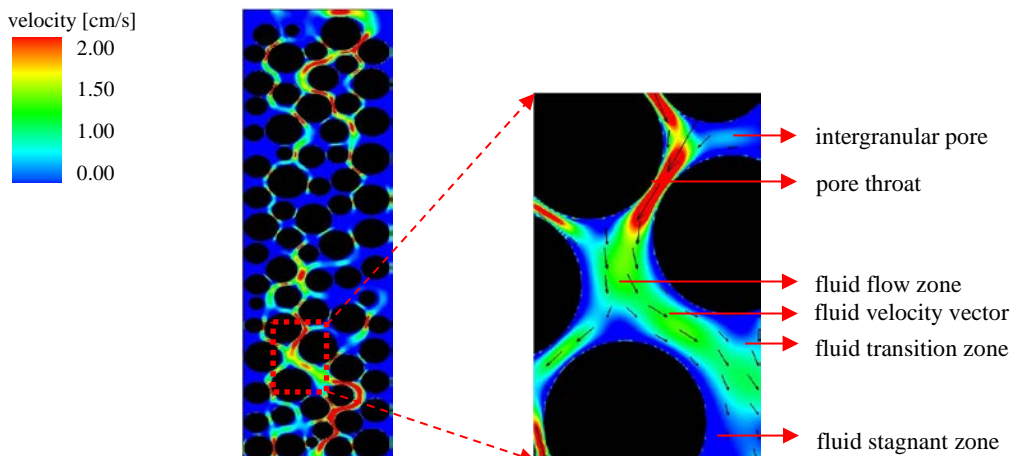


Fig. 8. Simulated flow velocity distribution inside the leaching column ($n = 35\%$, $Q = 0.5 \text{ mL/s}$)

5.3 Influence of irrigation rate on seepage velocity field

Irrigation rate is a variable that has been explored in heap leaching (Wu *et al.*, 2016; de Andrade Lima, 2006). In the actual leaching heap, the preferential flow and leaching blind regions easily form during the leaching process, and these negative factors have been revealed that to be relative to the irrigation rate and average porosity (Yin *et al.*, 2016) to a certain extent. In this work, three cases with three different spraying intensities, 0.3 mL/s , 0.4 mL/s and 0.5 mL/s , were simulated to investigate the effects of irrigation rate on fluid velocity. Figs. 9a, 9b and 9c depict the predicted seepage velocity fields for the abovementioned cases. It is evident that the main seepage channel, which is the seepage path of the preferential flow, exists in all the cases. In addition, with the increase in irrigation rate, the velocity of the fluid at the pore throat increases, and the main seepage channel branches gradually, this makes the preferential flow more obvious. Therefore, the irrigation rate has significant effects on the seepage velocity field, as

expected.

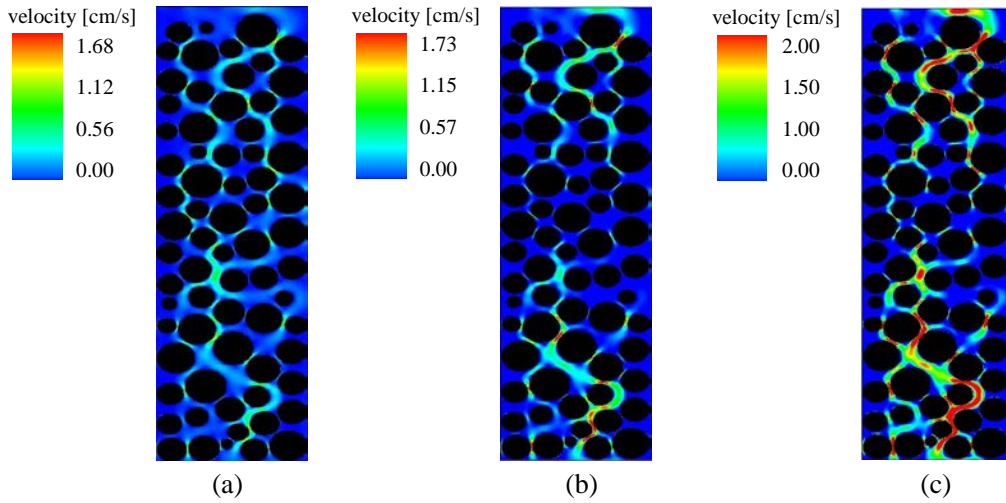


Fig. 9. Snapshots of the predicted seepage velocity field for different spraying intensities Q . (a) $Q=0.3$ mL/s, (b) $Q=0.4$ mL/s, (c) $Q=0.5$ mL/s. The porosity of the column heap is 35%.

The distribution of the seepage velocity is changed by the change in external conditions, and the seepage characteristics can be described by the percentage distribution of the fluid velocity. The comparison between the simulated fluid velocity distributions and the experimental results in the leaching column for the three different spraying intensities is shown in Fig. 10. In these three cases, the porosity of the column heap is 35%. It can be observed that the computational results are in good agreement with the experimental data, which suggests that the numerical approach taken in the current research is effective for studying the process of column leaching.

Based on the simulated results, when the irrigation rate are 0.3 mL/s, 0.4 mL/s and 0.5 mL/s, the corresponding velocity curves reach the maximum values of 0.142 cm/s, 0.284 cm/s and 0.336 cm/s respectively, and the maximum values are 1.68 cm/s, 1.73 cm/s and 1.99 cm/s, respectively. These results indicate that the distribution of the fluid velocity is similar and that low-velocity fluid fields dominate. The higher the velocity value is, the smaller the distribution is, although the irrigation rate is different. This is because the vortex field and the counter current are produced in the velocity field with the increase in irrigation rate, which reduces permeability in the vertical direction; thus the majority of the fluid domain has a low fluid velocity. On the other hand, the flow in the main seepage channel is dominated by gravity, and thus the preferential flow is easy to form. Consequently, the maximum fluid velocity is positively correlated with irrigation rate.

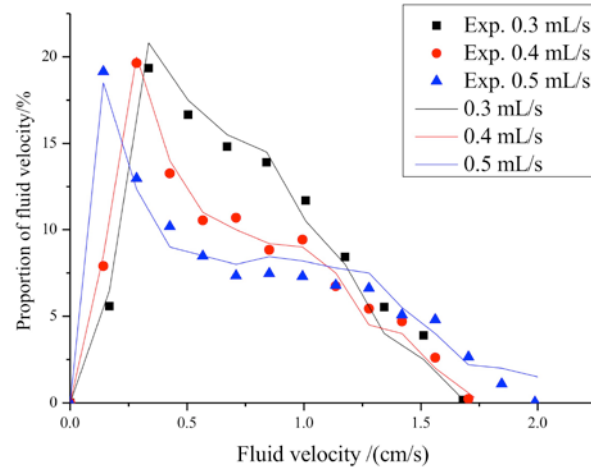


Fig. 10. Comparison of the simulated fluid velocity value distribution in leaching column for different spraying intensities with experimental data. The spraying intensities at the inlet are 0.3 mL/s, 0.4 mL/s and 0.5 mL/s, respectively. The porosity of column heap is 35%.

5.4 Influence of porosity on seepage velocity field

Porosity is defined as the volume fraction of pores and can be used to predict the permeability of flow (Lin *et al.*, 2005). To identify the influence of porosity on the seepage velocity field, the comparison of the predicted seepage velocity field in the leaching column for three different porosities is shown in Fig. 11. In addition, the irrigation rate at the inlet is set to be 0.5 mL/s. It is clearly observed that the fluid domains are still dominated by low-velocity flow in these three cases. Moreover, the porosities of the mesoscopic pore structure and the main seepage channel in the leaching column have changed. When the porosities of the column heap are 25%, 30% and 35%, the corresponding maximum fluid velocities at the pore throat are 1.70 cm/s, 1.85 cm/s, and 2.00 cm/s, respectively. Thus, under the same irrigation rate conditions, the maximum fluid velocity at the pore throat increases with the increase in porosity.

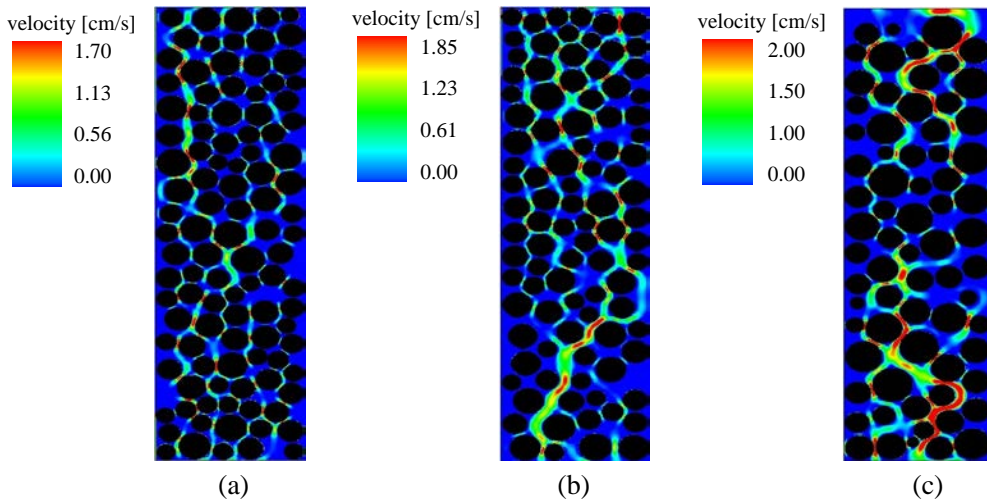


Fig. 11. Snapshots of the predicted seepage velocity field for different porosities n. (a) n=25%, (b) n=30%, (c) n=35%. The irrigation rate at the inlet is 0.5 mL/s.

The column heap is a discontinuous, heterogeneous and anisotropic bulk medium and the structural differences lead to different pore types and sizes. Hence, the porosity of a column heap has a significant influence on the saturated flow velocity. Fig. 12 illustrates the fluid velocity value distributions in the leaching column with different porosities. When the porosities are 25%, 30% and 35%, the corresponding peaks of the curves are obtained at 0.147 cm/s, 0.289 cm/s and 0.341 cm/s, respectively. It is well known that the flow in a packed leaching column depends on the geometric properties of the pore network structure and that the velocity field in the column heap is a complex dynamic field. From Fig. 11 and Fig. 12, it can be concluded that the connectivity between seepage channels and leaching solution permeability is poor under the condition of low porosity. This caused the local fluid velocity to increase rapidly and produce several fluid stagnant zones simultaneously. In contrast, in the case of high porosity, the seepage velocity field is no longer affected by microscopic forces such as surface viscous force, capillary suction and pore pressure. Therefore, it is easier to form the preferential flow that is gravitationally dominated. In this respect, increasing the porosity of a column heap appropriately can promote the formation of the preferential flow, causing the leaching solution to flow out of the leaching system through the main seepage channel directly, thereby decreasing the leaching rate.

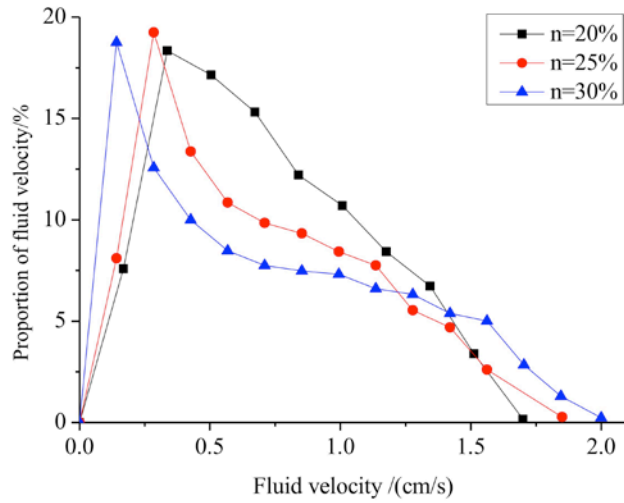


Fig. 12. Fluid velocity value distribution in leaching column with different porosities of the column heap. The irrigation rate at the inlet is 0.5 mL/s.

Even though we carry out some methods such as using agar to reduce noises of MRI images, there are some barriers of boundary limitations and other conditions during the simulating process. Our suggestion is that we could combine the actual leaching experiments with simulation, and modify the mathematical model based on actual experiments data, as a result, making and these simulating findings more dependable.

6. Conclusions

Based on the coupled DEM-LBM method, saturated flows in a column leaching are numerically investigated. The simulated results match the results of the corresponding MRI experiment well. Hence the approach proposed in this paper is feasible for simulating saturated flows in column leaching.

The main finding is that the main seepage channel exists along the high flow velocity region during the leaching process. Moreover, the microscopic seepage velocity field is mainly composed of the fluid stagnant zone, the fluid transition zone and the fluid flow zone. The fluid velocity vector profile shows that the fluid velocity increases when the fluid is close to the pore throat and the maximum fluid velocity is obtained at the center of the pore throat.

The seepage velocity field in a column heap exhibits a complex and dynamic state and is significantly affected by the irrigation rate and the porosity of the column heap. With the increase of the irrigation rate or the porosity, the preferential flow is easier to form, which is gravitationally dominated. However, the fluid domain is still dominated by low-velocity flow. The maximum fluid velocity is positively correlated with the irrigation rate and the porosity. Consequently, the interaction between the irrigation rate and the porosity affects the distribution of the fluid velocity.

Considering the limited properties of ore materials, it's hardly to realize imaging analysis by using the actual ores via MRI technology. Thus, it's not feasible to involve the leaching process and changes of ore shapes by using agar balls in this manuscript, and it's essential to figure out some valuable methods to reduce negative effect of ores and consider the multiphysics coupled effect during the MRI scanning in the future.

Acknowledgements

This work is financially supported by the National Key Research and Development Program of China (2016YFC0600704), the National Science Fund for Excellent Young Scholars (51722401), and the Key Program of National Natural Science Foundation of China (51734001).

References

- Cui, X., Li, J., Chan, A., & Chapman, D. (2012). A 2D DEM–LBM study on soil behaviour due to locally injected fluid. *Particuology*, 10(2), 242-252.
- Cundall, P. A. (1971). A computer model for simulating progressive, large scale movement in blocky rock systems. In Symp. ISRM, Nancy, France, Proc. (Vol. 2, pp. 129-136).
- Cundall, P. A. (1974). A Computer Model for Rock Mass Behavior using Interactive Graphics for the Input and output of Geometrical Data, Report Prepared under Contract Number DACW 45-74-c-006, for the Missouri River Division. US Army Corps of Engineers, University of Minnesota.
- de Andrade Lima, L. R. P. (2006). Liquid axial dispersion and holdup in column leaching. *Minerals engineering*, 19(1), 37-47.
- Fagan-Endres, M. A., Harrison, S. T., Johns, M. L., & Sederman, A. J. (2015). Magnetic resonance imaging characterisation of the influence of flowrate on liquid distribution in drip irrigated heap leaching. *Hydrometallurgy*, 158, 157-164.
- Fagan, M. A., Sederman, A. J., Harrison, S. T. L., & Johns, M. L. (2013). Phase distribution identification in the column leaching of low grade ores using MRI. *Minerals Engineering*, 48, 94-99.
- Feng, Y. T., Han, K., & Owen, D. R. J. (2007). Coupled lattice Boltzmann method and discrete element modelling of particle transport in turbulent fluid flows: Computational issues. *International Journal for Numerical Methods in Engineering*, 72(9), 1111-1134.
- Galindo-Torres, S. A. (2013). A coupled Discrete Element Lattice Boltzmann Method for the simulation of fluid–solid interaction with particles of general shapes. *Computer Methods in Applied Mechanics and Engineering*, 265, 107-119.
- Ghorbani, Y., Becker, M., Petersen, J., Morar, S. H., Mainza, A., & Franzidis, J. P. (2011). Use of X-ray computed tomography to investigate crack distribution and mineral dissemination in sphalerite ore particles. *Minerals Engineering*, 24(12), 1249-1257.
- Godel, B. (2013). High-resolution X-ray computed tomography and its application to ore deposits: From data acquisition to quantitative three-dimensional measurements with case studies from Ni-Cu-PGE deposits. *Economic Geology*, 108(8), 2005-2019.
- Han, Y., & Cundall, P. A. (2011). Lattice Boltzmann modeling of pore - scale fluid flow through idealized porous media. *International Journal for Numerical Methods in Fluids*, 67(11), 1720-1734.
- Han, K., Feng, Y. T., & Owen, D. R. J. (2007). Coupled lattice Boltzmann and discrete element modelling of fluid–particle interaction problems. *Computers & structures*, 85(11), 1080-1088.
- Jivkov, A. P., & Xiong, Q. (2014). A network model for diffusion in media with partially resolvable pore space characteristics. *Transport in porous media*, 105(1), 83-104.
- Johnson, D. H., Vahedifard, F., Jelinek, B., & Peters, J. F. (2017). Micromechanics of undrained response of dilative granular media using a coupled DEM-LBM model: A case of biaxial test. *Computers and Geotechnics*, 89, 103-112.
- Ke, C. H., Shu, S., Zhang, H., & Yuan, H. Z. (2017). LBM-IBM-DEM modelling of magnetic particles in a fluid. *Powder Technology*, 314, 264-280.
- Lin, C. L., Miller, J. D., & Garcia, C. (2005). Saturated flow characteristics in column leaching as described by LB simulation. *Minerals Engineering*, 18(10), 1045-1051.
- Lin, C. L., Videla, A. R., & Miller, J. D. (2010). Advanced three-dimensional multiphase flow simulation in porous media reconstructed from X-ray Microtomography using the He–Chen–Zhang Lattice Boltzmann Model. *Flow Measurement and Instrumentation*, 21(3), 255-261.
- Lin, Q. (2015). Use of X-ray Computed Microtomography to Measure the Leaching Behaviour of Metal Sulphide Ores.
- McBride, D., Cross, M., Gebhardt, J.E., (2012). Heap leach modeling employing CFD technology: A ‘process’ heap model. *Minerals Engineering* 33, 72-79.
- McBride, D., Ilankoon, I.M.S.K., Neethling, S.J., Gebhardt, J.E., Cross, M., (2017). Preferential flow behaviour in unsaturated packed beds and heaps: Incorporating into a CFD model. *Hydrometallurgy* 171, 402-411.
- Miao, X., Gerke, K. M., & Sizonenko, T. O. (2017). A new way to parameterize hydraulic conductances of pore elements: A step towards creating pore-networks without pore shape simplifications. *Advances in Water Resources*, 105, 162-172.
- Miao, X., Narsilio, G. A., Wu, A., & Yang, B. (2017). A 3D dual pore-system leaching model. Part 1: Study on fluid flow.

- Hydrometallurgy, 167, 173-182.
- Noble, D. R., & Torczynski, J. R. (1998). A lattice-Boltzmann method for partially saturated computational cells. International Journal of Modern Physics C, 9(08), 1189-1201.
- Owen, D. R. J., Leonardi, C. R., & Feng, Y. T. (2011). An efficient framework for fluid – structure interaction using the lattice Boltzmann method and immersed moving boundaries. International Journal for Numerical Methods in Engineering, 87(1 - 5), 66-95.
- Petersen, J. (2016). Heap leaching as a key technology for recovery of values from low-grade ores—A brief overview. Hydrometallurgy, 165, 206-212.
- Peskin, C. S. (2002). The immersed boundary method. Acta numerica, 11, 479-517.
- Videla, A. R., Lin, C. L., & Miller, J. D. (2008). Simulation of saturated fluid flow in packed particle beds—The lattice-Boltzmann method for the calculation of permeability from XMT images. Journal of the Chinese Institute of Chemical Engineers, 39(2), 117-128.
- Videla, A. R., Matamala, L. F., Uribe, S., Andia, M. E. (2016). Ferrous Ion oxidation monitoring by using magnetic resonance imaging for bio-oxidation laboratory testing. Minerals Engineering, 106(5): 108-115.
- Wang, L., Zhang, B., Wang, X., Ge, W., & Li, J. (2013). Lattice Boltzmann based discrete simulation for gas–solid fluidization. Chemical Engineering Science, 101, 228-239.
- Wildenschild, D., & Sheppard, A. P. (2013). X-ray imaging and analysis techniques for quantifying pore-scale structure and processes in subsurface porous medium systems. Advances in Water Resources, 51, 217-246.
- Wu, A. X., Chao, L. I. U., Yin, S. H., Xue, Z. L., & Xun, C. H. E. N. (2016). Pore structure and liquid flow velocity distribution in water-saturated porous media probed by MRI. Transactions of Nonferrous Metals Society of China, 26(5), 1403-1409.
- Yin, S. H., Wang, L. M., Chen, X., Wu, A. X. (2016). Effect of ore size and heap porosity on capillary process inside leaching heap. Transaction Nonferrous Metal Society of China 26, 835-841.
- Yin, S. H., Wang, L. M., Kabwe, E., Chen, X., Yan, R. F., An, K., Zhang, L., Wu, A. X. (2018). Copper Bioleaching in China: Review and Prospect. Minerals 8, 32.
- Yin, S.H., Wang, L.M., Wu, A.X., Kabwe, E., Chen, X., Yan, R.F., (2018). Copper recycle from sulfide tailings using combined leaching of ammonia solution and alkaline bacteria. Journal of Cleaner Production 189, 746-753.
- Yang, B. H., Wu, A. X., Miao, X. X., & Liu, J. Z. (2014). 3D characterization and analysis of pore structure of packed ore particle beds based on computed tomography images. Transactions of Nonferrous Metals Society of China, 24(3), 833-838.